Radiation Measurements 175 (2024) 107155

Contents lists available at ScienceDirect

Radiation Measurements

journal homepage: www.elsevier.com/locate/radmeas

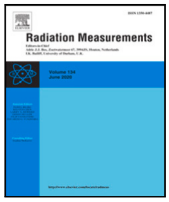

Durolon® polymer as a nuclear track detector: Characterization by chemical etching

K.C.C. Pires [a,*], Y. Abuchaim [a,1], R. Künzel [b], S. Guedes [c], M. Assunção [b], N.M. Trindade [a], R.R. Aquino [d], O.C.B. Santos [a]

[a] Departamento de Física Nuclear, Instituto de Física, Universidade de São Paulo, 05508-090, São Paulo, Brazil
[b] Departamento de Física, Universidade Federal de São Paulo, Campus Diadema, 09972-270, São Paulo, Brazil
[c] Instituto de Física Gleb Wataghin, Universidade Estadual de Campinas, 13083-859, São Paulo, Brazil
[d] Laboratório de Radiometria Ambiental, Instituto de Pesquisas Energéticas e Nucleares, 05508-000, São Paulo, SP, Brazil

ARTICLE INFO

Keywords:
Durolon®
Alpha particle
Nuclear tracks
Etch pits
Chemical etching
UV–vis spectroscopy
Raman spectroscopy

ABSTRACT

This paper presents the properties of alpha particle tracks in a polymer, known as Durolon®. The study involves measurements of the time-dependent evolution of etch pit diameters and areal densities for low-energy alpha particles under various etching conditions, including different temperatures and solutions. A time-dependent model was successfully employed to describe the etch pit growth rates. Additionally, optical absorption and Raman spectroscopy techniques were applied to the samples under investigation, complementing the traditional results obtained through optical microscopy. The suitability of Durolon® polymer as a nuclear track detector is discussed based on the results obtained from the aforementioned complementary techniques. In summary, this research represents a critical step toward establishing Durolon® polymer as a viable nuclear track detector.

1. Introduction

Durolon®is a trade name used to identify various high-performance polymers that have superior mechanical and thermal properties compared to many other materials. It is a commercial bisphenol-A polycarbonate ($C_{15}H_{16}O_2$) commonly utilized in applications requiring high strength, durability, and toughness (Durolon, 2009; Araújo et al., 1998). Durolon®exhibits high heat resistance, characterized by its elevated softening temperature (T_m = 225 °C), high glass transition temperature (T_g = 140–150 °C), and melting point ranging from 230 to 270 °C (Freitag et al., 1988; Chen et al., 2005; Artham and Doble, 2008; Delpech et al., 2002). It is also an amorphous material with favorable physical and chemical properties (Silva et al., 2024). Due to these characteristics, it has been considered for use as a nuclear track detector (NTD) to investigate the characteristics of alpha particle etch pits (Pugliese, 2008).

When a charged particle, such as an alpha particle, penetrates a polymer, it creates a damaged trail within the material known as a latent track. This track is typically several micrometers long and a few nanometers in diameter. After undergoing chemical etching, a conical channel with a diameter in the range of tens of micrometers is formed around the latent track, which can be observed using an optical microscope. The two-dimensional projection of this channel from a top-down view is referred to as the etch pit. The observed diameters and grayscale levels of the etch pits are correlated with the energy and incident angle of the alpha particles (Pugliese, 2008; Knoll, 2010).

Understanding the etching dynamics of the pits is crucial for interpreting results obtained under various conditions, such as radiation exposure, chemical etching solutions, and temperature variations. Furthermore, this understanding facilitates the identification of conditions that provide more satisfactory etching for specific applications. This study aims to investigate the dynamics of low-energy alpha particle track in Durolon®samples using two chemical etching solutions, namely NaOH and KOH, at temperatures of 70 and 80 °C. Additionally, a phenomenological model is proposed to accurately describe the growth of etch pit diameters. To characterize the polymer structure, measurements were performed using optical absorption and Raman spectroscopy techniques. Both UV–vis and Raman spectroscopy techniques are non-destructive and provide complementary information about the chemical and physical changes induced by alpha radiation exposure. They offer valuable tools for characterizing and understanding the radiation-induced effects on the Durolon®polymer.

The article is organized as follows. Section 2 outlines the procedures employed for ^{241}Am alpha source irradiation, chemical etching, and

* Corresponding author.
E-mail address: kelly@if.usp.br (K.C.C. Pires).
[1] Present address: Instituto de Astronomia, Geofísica e Ciências Atmosféricas, Universidade de São Paulo, São Paulo, Brazil.

https://doi.org/10.1016/j.radmeas.2024.107155
Received 23 December 2023; Received in revised form 1 May 2024; Accepted 3 May 2024
Available online 7 May 2024

Fig. 1. Photograph of the experimental setup used to irradiate the Durolon® polymers and the CR-39 detectors previously studied (Oliveira et al., 2021). The lead castle is located in the center, while the cover where the detectors were fixed is on the left. On the right is the ^{241}Am alpha source.

sample visualization under the microscope. The Semi-Empirical Model for describing the results of track growth considering the etching velocity and bulk etching velocity ratio is detailed in Section 3. In Section 4, the analysis of etch pit diameter growth utilizing the proposed model, the response of etch pit densities, as well as Ultraviolet–visible (UV–vis) and Raman spectroscopy measurements are presented. Concluding remarks are provided in Section 5. This paper carries new information on alpha particle track etching. It is worth mentioning that we have adequately employed the conclusions of previous studies on alpha particle track detection and measurement (for instance, Rana (2008), Dörschel et al. (1999), Rana (2010), Fromm et al. (1988)) in the present paper.

2. Materials and methods

The Durolon® polymer utilized in this study was manufactured by the Brazilian company Unigel Plásticos S/A and distributed by Incomplast (Cassou and Benton, 1978; Durolon, 2009). It exhibits an approximate transmittance of 89%, high electrical resistivity (greater than $10^{16}\Omega$cm), and can support traction of up to 68 MPa (Durolon, 2009). The polymer samples, with 0.814 ± 0.003 mm thickness, were cut into 1 × 1 cm pieces. Subsequently, the samples were irradiated with 5.5 MeV alpha particles emitted from a calibrated ^{241}Am source, with an activity of 1000 alpha particles per second, for a total duration of 6.5 h. The source was manufactured at the Nuclear and Energy Research Institute (São Paulo, Brazil). The source distance to the surface detector was 41.36 μm in all experiments. The irradiation was conducted alongside CR-39 type detectors that had been previously studied (Oliveira et al., 2021), as shown in Fig. 1, enabling a precise comparison between both detectors in the future. The incidence energy of the alpha particles on the detector surface was estimated taking advantage of the spectrometric properties of etch pit diameter and gray level (Soares et al., 2013). Two pieces of CR-39 irradiated with alpha particles from a ^{241}Am source at two different source-detector distances (29.15 ± 0.46 mm and 41.36 ± 0.18 mm) were etched together under standard conditions (NaOH, 6.25 M, for 400 min at 70 °C), and their diameters were measured. Subsequently, using a curve of the product of diameters as a function of alpha particle energy from Ref. Soares et al. (2013), the energies of the alpha particles were estimated. The alpha particles in the detector exposed at a distance of 41.36 ± 0.18 mm, the ones analyzed in the present paper, were found to have an energy of 1.5 ± 0.5 MeV. Although the method is relatively accurate, the value found is not very precise. Due to this limitation, we preferred to base our analysis on the energy range of 1–2 MeV, rather than pointing to a specific value.

In the present study, the irradiated detectors were etched using two solutions with different mass percentages of each reagent in their respective fractions: 15% KOH (or NaOH), 40% C_2H_6O (ethyl alcohol), and 45% high-purity water. Chemical etching was performed in 15-minute steps, with the detectors fully immersed in the solutions, which

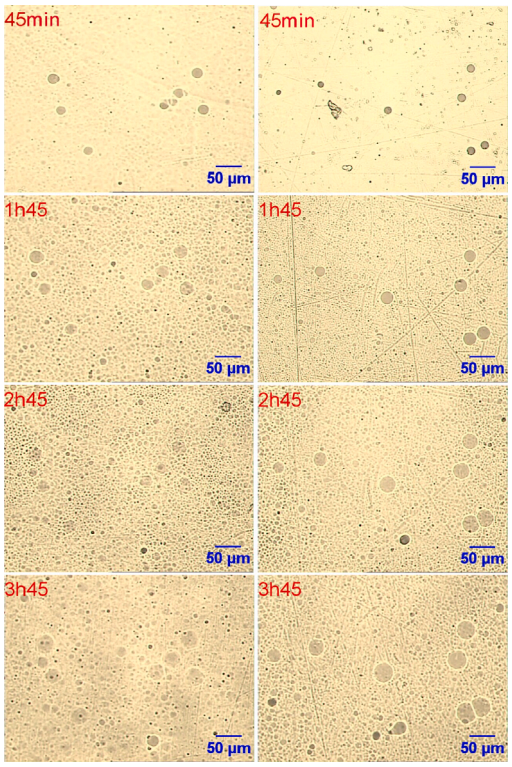

Fig. 2. Typical images of the Durolon® samples etched at 70 °C with NaOH (left) and KOH (right) solutions at different etching time steps.

were maintained at a constant temperature of either 70 or 80 °C. To prevent evaporation during the operation, the beakers were covered with plastic film. After each etching step, the detectors were transferred to a solution of nitric acid (HNO_3, 2.3 M) to stop the etching process. Upon completion, the samples were washed with deionized water, left to air dry, and stored.

Etch pits were identified and observed using a Leitz Diaplan optical microscope. Images were captured using a camera attached to the microscope and processed using the computer code *Leica Qwin* with a magnification of 78.75×. The analysis of the images was carried out using the *ImageJ* code (Ferreira and Rasband, 2012). The same set of etch pits was monitored in specific regions of the detectors after each etching step, for approximately 5 h in the case of KOH solution and approximately 2.5 h for NaOH solution. These regions were randomly selected but spaced apart to ensure a better sampling of the etch pits over the detector surface.

The exposition geometry limits the incidence angle of the alpha particles on the detector surface. As a consequence, after etching, the etch pits appeared as roundish figures. No stretched ellipses-like pits are observed. For the analysis of etch pit growth, the incidence angle was further limited. Only pits formed by alpha particle tracks incident nearly perpendicularly to the surface were selected (with a minor and major pit diameters ratio larger than 0.7). Fig. 2 displays examples of etch pit evolution obtained using NaOH (left) and KOH (right) solutions at different etching time steps at 70 °C.

Following each etching experiment, the diameters of the etch pits were measured, and the average value was calculated by considering all monitored etch pits within the selected regions for each etching time. Step-etch curves were obtained for both chemical solutions (KOH and NaOH) at different etching temperatures: 70 and 80 °C. The results, along with data uncertainties represented by the standard deviation, are presented in Fig. 3. The standard deviation was calculated taking into account the multiple diameter measurements obtained from the pre-selected monitored regions.

A phenomenological model based on a proposed track velocity profile was applied to describe the experimental data. A detailed discussion of this model will be provided in Section 3. The etch pit density curves for both chemical solutions and temperatures were also investigated, revealing a significant decrease in density for both cases.

Additionally, experimental measurements using UV–visible (UV–vis) and Raman spectroscopy techniques were performed. Raman spectroscopic measurements were carried out within the range of 200–2000 cm^{-1}, employing a Raman Renishaw microscope (InVia) equipped with a multi-channel charge-coupled device (CCD), an 830 nm excitation laser, and a grating system with 1200 l/mm. The data were registered using the automatic cosmic ray removal option. The wavenumber calibration of the Raman spectra was accomplished using the characteristic silicon line observed at approximately 520.4 cm^{-1}. A fifth-order polynomial baseline was applied to subtract the background signal from the raw experimental Raman spectrum. UV–vis spectra were obtained in absorbance mode, ranging from 300 to 800 nm, using a Shimadzu 2600 series UV–vis spectrophotometer with a sampling interval of 0.2 nm. The absorbance measurements were performed at room temperature, with air serving as the reference material.

3. Semi-empirical model

Durolon®is a polycarbonate ($C_{16}H_{14}O_3$) with a density of 1.15 g/cm^3. A Monte Carlo simulation was conducted using the TRIM code to determine the penetration of alpha particles with energies between 1–2 MeV in the detector material. The resulting value indicated a depth of 4.6–9.41 μm. To fit the experimental data, the sensitivity function $V(t) = v_t(t)/v_b$ was utilized, where $v_t(t)$ represents the etching velocity in the track direction, and v_b corresponds to the bulk etching velocity. This sensitivity function was modeled as a constant with a smooth transition to 1 ($v_t \rightarrow v_b$) at the end of the track. When a 1–2 MeV alpha particle hits the detector (Durolo®sample), its stopping power is near the Bragg peak, and as it slows down, the energy deposition gradually decreases until the particle comes to a stop. The mathematical representation of this model is a piecewise function:

$$V(t) = \begin{cases} V_0 & \text{if } t \leq \tau + \epsilon \\ \frac{t+\tau}{t-\tau} & \text{if } t > \tau + \epsilon \end{cases} \quad (1)$$

where t represents the variable for the etching time, τ denotes the etching time at which V starts transitioning to 1 ($v_t \rightarrow v_b$), and ϵ represents a time increment necessary for the continuity of $V(t)$. The value of ϵ is determined as:

$$\epsilon = \frac{2\tau}{V-1}, \quad (2)$$

At the time τ, the depth of the track aligns with the etchable track length, taking into account the removed layer of the detector. The relationship between the etch pit diameter and the track and etching velocities for tracks created by alpha particles incident perpendicular to the observation surface is described by Somogyi and Szalay (1973) as follows:

$$D = 2v_b t\sqrt{\frac{V-1}{V+1}} = \begin{cases} 2\beta v_b t\sqrt{\frac{V_0-1}{V_0+1}} & \text{if } t \leq \tau + \epsilon \\ 2\beta v_b \sqrt{\tau}\sqrt{t} & \text{if } t > \tau + \epsilon \end{cases} \quad (3)$$

Eq. (3) is obtained by substituting the model for V shown in Eq. (1). This equation predicts an initial linear growth in track diameter, followed by a transitional period where the curve changes slope as the etching velocity in the track direction approaches v_b ($V(t) \rightarrow 1$), in which tracks enter the spherical regime. The scale factor β, ideally set to $\beta = 1$, was introduced to enable comparison with experimental data. The proposed model is based on the traditional modeling of track diameters in isotropic solids (Somogyi and Szalay, 1973), in which the track etch velocity is variable. We only proposed a new V-function.

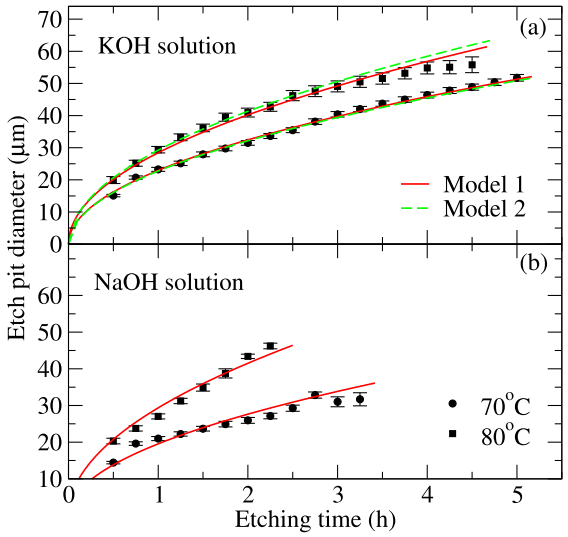

Fig. 3. Etch pit diameters, along with their associated uncertainties quantified by the standard deviation, versus etching time for Durolon®sample using (a) KOH and (b) NaOH solutions at 70 °C (circles) and 80 °C (squares). The red solid line is the fitting using the Eq. (4). The dashed green line represents a test fit conducted using the same equation, but an identical number of data points for both KOH and NaOH solutions (Model 2).

4. Results and discussion

Fig. 3 presents the etch pit diameters versus etching time for Durolon®sample using different chemical solutions and temperatures, with data uncertainties represented by the standard deviation. The trends observed in the diameter variation shown in Fig. 3 suggest that the data for lower etching times are already within the transitional time range.

To fit the data, the product $2\beta v_b\sqrt{\tau}$ from Eq. (3) can be replaced with a constant c to simplify the equation:

$$D(t) = c\sqrt{t} \quad (t > \tau + \epsilon) \quad (4)$$

As defined in Eq. (4), parameter c is proportional to v_b. Also, Eq. (4) holds for tracks in the spherical regime ($t > \tau + \epsilon$). To simultaneously fit the data etched at 70 °C and 80 °C for each solution, the parameter c was modified to be a linear function of the etching temperature (T), expressed as $c = (a + bT)$, where T is measured in Celsius degrees.

The Eq. (4) was adjusted to the experimental data, and the results of the fitting are represented by a solid red line in Fig. 3 (Model 1). The fitted parameters, as well as the value of c calculated from parameters a and b, are shown in Table 1.

Since parameter c is proportional to bulk etch velocity, it can be used to compare the effects of the different etching conditions on v_b. For both etching reagents, KOH and NaOH, the value of the parameter c for 80 °C is higher than for 70 °C experiments (Table 1). Comparing between reagents, the parameter c presents a higher value for KOH for experiments carried out at 70 °C. However, for the 80 °C experiment, there is an inversion and the value of c is higher when NaOH is the chemical reagent. To investigate the impact of varying the number of data points in the etching experiments on the fitting parameters, we repeated the fitting procedures using an identical number of data points, referred to as Model 2. Although there was a change in parameter c, it did not alter the observed inversion in the value of this parameter from Model 1 (see values in parentheses in Table 1).

This result can be analyzed in terms of the Arrhenius activation energy, which is associated with the rate constants and, consequently, with the bulk etching velocities of the studied etching processes (Cohen et al., 2007). The Arrhenius activation energy, as defined by

Table 1
Parameters of Eq. (4) fitted to experimental data using the Semi-Empirical Model. The values in parentheses represent the obtained fitting parameters achieved using the same equation but considering an equal number of points for both solutions, denoted as Model 2.

Etching solution	Temperature (° C)	a(μm/h$^{1/2}$)	b (μm/(h$^{1/2}$ °C))	c(μm/h$^{1/2}$)	χ^2
KOH	70 80	−15.41 (−22.62)	0.542 (0.648)	22.53 (22.74) 27.95 (29.22)	1.23 (1.06)
NaOH	70 80	−49.18	1.007	21.31 31.38	6.10

The values of c are also shown in the table.

the International Union for Pure and Applied Chemistry (IUPAC), accounts for variations in activation energies based on temperature and specific characteristics of chemical reactions (Aquilanti et al., 2010). The inversion observed in the v_b values associated with NaOH and KOH suggests that at least one (and possibly both) of the activation energies changes with temperature. Specifically, the activation energy for etching with NaOH becomes smaller than the activation energy for KOH etching as the etching temperature increases. An in-depth exploration of the temperature dependence of the activation energy would require conducting etching experiments across a broader range of temperatures – an avenue for future research.

In a previous study (Pugliese, 2008), Durolon® was used as a detector for 1.47 MeV alpha particles and 840 keV ^{7}Li recoil emitted by the ^{10}B(n, α)^{7}Li reaction. The authors determined the bulk etching velocity, v_b, to be 8.64 μm/h for etching with a solution containing the same concentrations of NaOH, ethyl alcohol, and water used in this work, at a temperature of 70 °C. This value of v_b is in the same magnitude of values reported for Makrofol, which is also a polycarbonate material (Balestra et al., 2007). The previous study examined etch pit diameter growth in Durolon® for etching times up to 25 minutes, during which the diameters increased linearly. The data presented in the current work corresponds to etching times beyond 25 min and appears to be in the transitional time range of V. Therefore, for the analysis, it is assumed that $\tau \approx 25$ min. As is going to be shown below, this value is an underestimation for the detector we are studying. An analysis of the track diameters indicates that the value of v_b should be about twice the picked value.

Using the values from Table 1, the expression $2\beta v_b\sqrt{\tau}$ yields a value of 21.3 μm/h$^{1/2}$ for the 70 °C NaOH etching. With v_b = 8.64 μm/h, we find β=1.9, which is considerably higher than the ideal value of 1. One possible explanation is an underestimation of the value of v_b taken from the literature. Setting $\beta = 1$, the value obtained for bulk etch velocity would $v_b \approx 16.2$ μm/h, which is more compatible with the etch pit diameter values measured in this study. For instance, after 30 min, the track diameter would be about 16 μm, close to the value found for the curve representing etching at 70 °C in Fig. 3.

Another possible effect contributing to this higher value of β is that the semi-empirical model was initially developed based on the assumption that the diameter measurements were limited to etch pits formed by tracks of normal incidence. However, the measurements in this study were carried out with a less restrictive criterion (diameter ratio > 0.7). Therefore, to some extent, β serves as an indicator of the angular spread of the measured tracks.

Indeed, the model for the track profile described in this work is semi-empirical because it still involves an adjustable parameter, β, that has to be adjusted to make the predicted curve compatible with the experimental data on the etching time dependence of track diameter growth. In addition to the angular spread of the incidence angle of the tracks considered for measurement, the slow v_t transition toward v_b also contributes to the higher-than-expected value of β. The V-function tends to but remains higher than 1 for the entire range of data. On average, it is conservatively estimated that this effect is less than 25%. However, the semi-empirical model does offer the possibility to estimate the value of a parameter if the others are measured. For example, if v_b is measured and τ is estimated from a diameter growth curve starting with shorter etching times, the track etching velocity, v_t, can be estimated. Future work can focus on improving the modeling of the V function by exploring smoother functions to represent the transition of v_t to v_b during etching. This could potentially provide a more accurate representation of the experimental data and further refine the estimation of parameters.

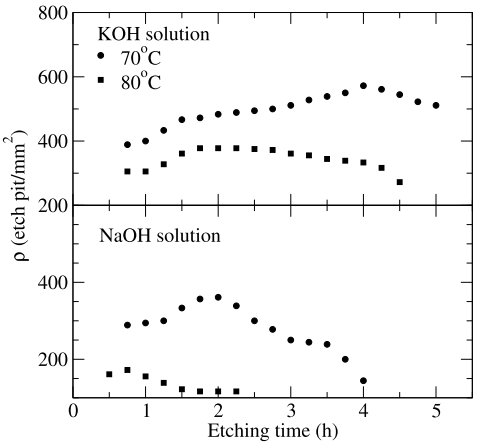

Fig. 4. Etch pit densities obtained for the Durolon® polymer etched with the KOH (top) and NaOH (bottom) solution versus etching time.

4.1. Superficial densities of etch pits

The experimental setup used in this study provided precise control over the distance between etch pits, enabling accurate measurements of their diameters, as shown in Fig. 2. Due to this precise control, relying solely on Poisson uncertainties would be inadequate for estimating the uncertainties in etch pit counts at different etching stages. Therefore, uncertainties in the calculation of etch pit densities were neglected in this analysis. The regions where etch pits were counted and measured remained constant during all experiments (see Fig. 2), ensuring uniformity. Consequently, we estimated the uncertainties in etch pit densities at 8%, focusing solely on systematic uncertainties related to area determination.

Fig. 4 presents the curves of mean superficial densities of etch pits obtained after each etching experiment. These curves provide valuable information about the evolution of etch pit density as a function of etching time and the type of chemical solution used.

The observed behavior of etch pit densities, such as the rapid increase followed by a plateau or decrease, can be attributed to the penetrability of low-energy alpha particles in the polymer. The alpha particle penetration depth in the polymer was determined to be in the range of 4.61–9.41 μm (Oliveira et al., 2021). For the KOH solution, the etch pit densities increase rapidly and then become nearly constant before decreasing. This behavior suggests that the low-energy alpha particles create superficial tracks that are not fully developed and are quickly erased during the chemical etching process. As a result, the etch pit densities reach a plateau as the etching removes the superficial tracks but leaves behind the deeper, more well-developed tracks. In contrast, for the NaOH solution, a reduction in etch pit densities is

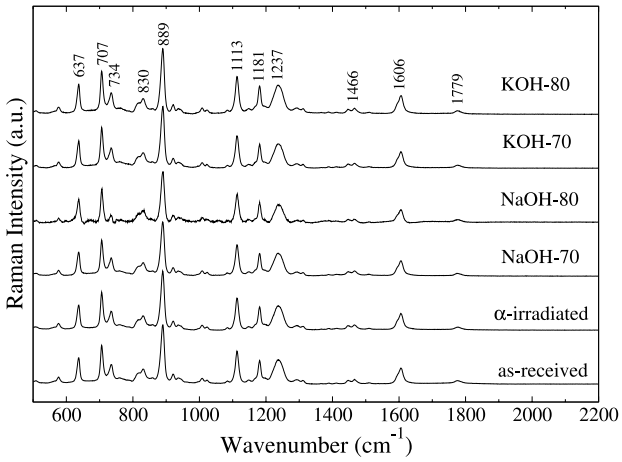

Fig. 5. Raman spectra from as-received and the α-irradiated Durolon® sample compared with samples submitted to different chemical etching treatments and temperatures.

observed with an increase in etching time. This behavior indicates that the low-energy alpha particles create superficial tracks that are easily erased during the etching process. As the etching progresses, the erasure of these superficial tracks leads to a decrease in etch pit densities. Overall, the observed behavior of etch pit densities reflects the different penetrability of low-energy alpha particles in the polymer and the extent to which the tracks are developed during the etching process.

4.2. Raman and UV-vis spectroscopy

The effect of alpha radiation exposure on the chemical and physical properties of Durolon® polymer was investigated using UV–vis and Raman spectroscopic techniques. These spectroscopic measurements provide valuable insights into the changes occurring at the molecular level and can reveal alterations in the polymer's structure and composition.

Raman spectroscopy is a highly effective technique for investigating the chemical and structural properties of polymeric materials and for identifying microstructural modifications induced by radiation exposure and chemical etching solutions. It provides valuable insights into the molecular composition, bonding, and vibrational modes of the material. Fig. 5 shows the Raman spectra obtained from the as-received sample and the sample solely exposed to irradiation, and provides a comparison with the irradiated Durolon® samples subsequently etched with different chemical solutions (NaOH and KOH) at temperatures of 70 °C and 80 °C. The wavenumber uncertainty of the Raman spectra is around 0.55 cm^{-1}. The registered Raman spectra presents the characteristic peaks of polycarbonate and reveals prominent bands, which are identified in the mentioned figure, and detailed assignments can be found in Table 2.

The Raman spectra of Durolon® (Fig. 5) exhibits distinct bands associated with specific molecular vibrations. Notably, the prominent peaks correspond to ring and/or C–H vibrations at 734, 830, and 1606 cm^{-1}, while the C=O stretching vibration appears at 1777 cm^{-1}. The Raman band observed at 889 cm^{-1} is related to the vibrations of the O–(C=O)–O and/or ν(C–CH3) group.

The registered Raman profiles indicate that the spectra of the as-received, irradiated, and etched samples exhibit similar bands. The data in Fig. 5 are normalized to unit area. The Raman bands occur at similar wavenumbers as those observed in the as-received detector, as illustrated in Table 3. These findings suggest that the detectors submitted to irradiation and etching processes at the temperatures employed in this study did not exhibit phase changes or significant modifications in their bond lengths.

The Full Width at Half Maximum (FWHM) of prominent Raman bands were utilized to assess the degree of disorder in the studied polymers (Pelletier, 2003). A ordered material typically exhibits sharper and narrower Raman lines compared to an amorphous material (Dybal et al., 1998). Table 3 presents the FWHM values for the most prominent Raman peaks observed in the registered spectra. The FWHM were calculated by fitting a Gaussian profile to each peak listed in Table 3. The table illustrates that when the polymer is submitted to irradiation and etching, its ordering degree tends to decrease, indicating an increase in disorder. The results also indicate varying degrees of disorder among the detectors, with the samples subjected to etching at 80 °C displaying higher levels of disorganization.

The intensity ratios of the 889 cm^{-1} (O-(C=O)-O), 1237 cm^{-1} (C-O), and 734 cm^{-1} (C-H) bands in relation to the 1604 cm^{-1} band (associated with the phenyl ring) were calculated to evaluate the effect of the alpha particle irradiation and etching at different temperatures on the spectral bands from the same dataset. The results are summarized in Table 4. It is evident from the results that the intensity ratios of the 889 cm^{-1}/1604 cm^{-1} and 127 cm^{-1}/1606 cm^{-1} bands exhibit only minor variations in spectra obtained from the irradiated and etched samples when compared to the spectra from the as-received sample. However, there is an increase in the 734 cm^{-1}/1604 cm^{-1} ratio for the etched and irradiated samples. These results suggest that the irradiation of Durolon® with low-energy alpha particles and the etching process mainly affect the C-H group.

UV–vis absorbance measurements were carried out to investigate the presence or absence of chromophore groups in the Durolon® polymer resulting from irradiation or a combination of irradiation and chemical etching processes. The UV–vis optical absorption spectra obtained for the Durolon® samples under various conditions are presented in Fig. 6. The estimated uncertainty in the wavelength from the UV–vis measurements corresponds to approximately 0.1 nm.

Fig. 6 illustrates that the as-received, irradiated, and etched samples display a similar absorbance profile ranging from 300 to 800 nm. In terms of UV–vis emission intensity, the results indicate that the irradiated and etched samples at 70 °C exhibit higher absorption, while the irradiated sample shows lower absorption intensity compared to the as-received detector. For the samples submitted to etching processes at 80 °C, the absorbance intensity is comparable to that observed in the as-received sample. The changes in absorbance intensity can be attributed to differences in sample thickness, structure, and chemical composition induced by the irradiation and etching processes. The thickness of each sample was measured at several positions over the detectors, providing the following medium values: 1.020(19) mm (as-received), 1.008(14) mm (alpha-irradiated), 0.816(6) nm (KOH-70), 0.696(18) mm (KOH-80), 0.7416(25) mm (NaOH-70), and 0.6489(28) mm (NaOH-80). While a significant reduction in the thickness of the irradiated detectors is observed when etched at both 70 °C and 80 °C, their absorbance increases, suggesting potential modifications in their chemical composition and/or structure. These changes are likely a result of main chain scission and cross-linking effects (Rahaman et al., 2014).

The transparency of amorphous polymers, including Durolon®, is a desirable characteristic that can be influenced by exposure to ionizing radiation, leading to changes in the atomic structure of the material (Gupta et al., 2015). In this study, the irradiated samples exhibited a transparent appearance, which is supported by their nearly zero absorbance in the visible region of the spectrum. The potential impact on the transparency of the polymer samples was assessed by determining the band gap. As shown in Fig. 6, a slight shift in the absorption edge was observed for the samples subjected to irradiation or chemical etching, indicating a minor variation in the band-gap value. The Tauc equation (Wood and Tauc, 1972) was employed to calculate the optical band-gap of the Durolon® polymer for direct allowed transitions, and the results are presented in Table 5. The Jacobian conversion

Table 2
Assignment of the prominent Raman bands observed in the Durolon® spectra.

Wavenumber (cm^{-1})	Assignment	Reference
637	phenyl ring deformation	Gedler et al. (2013), Liu et al. (1990)
707	ring deformation	Gedler et al. (2013)
734	C-H wag	Zimmerer et al. (2019), Gedler et al. (2013)
830	phenyl ring vibration	Lee et al. (2000), Stuart (1996)
	C-H wag	Resta et al. (2015), Gedler et al. (2013)
889	ν[O-(C=O)-O]	Zimmerer et al. (2019), Stuart (1996)
	ν(C-CH3)	Gedler et al. (2013)
1113	β(CH) ring, CH wag	Zimmerer et al. (2019), Lee et al. (2000)
	CH wag	Gedler et al. (2013), Resta et al. (2015)
1181	CH wag	Lee et al. (2000)
1237	C-O stretch, νas(C-O-C), δ(CO)	Zimmerer et al. (2019)
1466	CH3 deformation, CH3 asymmetry	Stuart (1996), Resta et al. (2015)
	CH3 asymmetric bend	Zimmerer et al. (2019)
1606	ring stretch	Lee et al. (2000), Gedler et al. (2013)
1779	ν(C=O)	Stuart (1996), Gedler et al. (2013) Zimmerer et al. (2019)

Table 3
The FWHM and centroid values for the most prominent Raman peaks.

Detector	Raman Band (cm^{-1})							
	1606		1237		889		734	
	FWHM (cm^{-1})	Centroid (cm^{-1})	FWHM (cm^{-1})	Centroid (cm^{-1})	FWHM (cm^{-1})	Centroid (cm^{-1})	FWHM (cm^{-1})	Centroid (cm^{-1})
as-received	20.17 ± 0.33	1604.4	33.35 ± 0.33	1237.3	12.54 ± 0.33	889.2	11.7 ± 0.9	734.6
irradiated	20.23 ± 0.34	1604.3	33.28 ± 0.34	1237.3	12.44 ± 0.32	889.1	11.8 ± 0.9	734.6
KOH-70	20.00 ± 0.39	1604.4	33.45 ± 0.39	1237.4	12.62 ± 0.32	889.2	11.6 ± 0.9	734.6
KOH-80	20.42 ± 0.36	1604.3	33.13 ± 0.36	1237.2	12.60 ± 0.34	889.1	12.1 ± 0.9	734.5
NaOH-70	20.1 ± 0.4	1604.2	33.8 ± 0.4	1237.1	12.57 ± 0.32	889.1	12.1 ± 0.9	735.5
NaOH-80	20.6 ± 0.6	1604.8	33.5 ± 0.6	1238.3	12.72 ± 0.36	889.5	12.2 ± 0.9	734.5

Table 4
Illustration of the Raman band intensity ratios calculated for bands in the same spectrum. The number in parenthesis corresponds to the percentage of the ratio for the as-received detector.

	as-received	irradiated	NaOH-70	NaOH-80	KOH-70	KOH-80
I(889)/I(1606)	3.76 (100)	3.84 (102)	3.62 (96)	3.78 (101)	3.90 (104)	3.68 (98)
I(1237)/I(1606)	1.55 (100)	1.59 (103)	1.52 (98)	1.54 (99)	1.59 (103)	1.58 (102)
I(734)/I(1606)	1.35 (100)	1.41 (104)	1.38 (102)	1.49 (110)	1.49 (110)	1.52 (113)

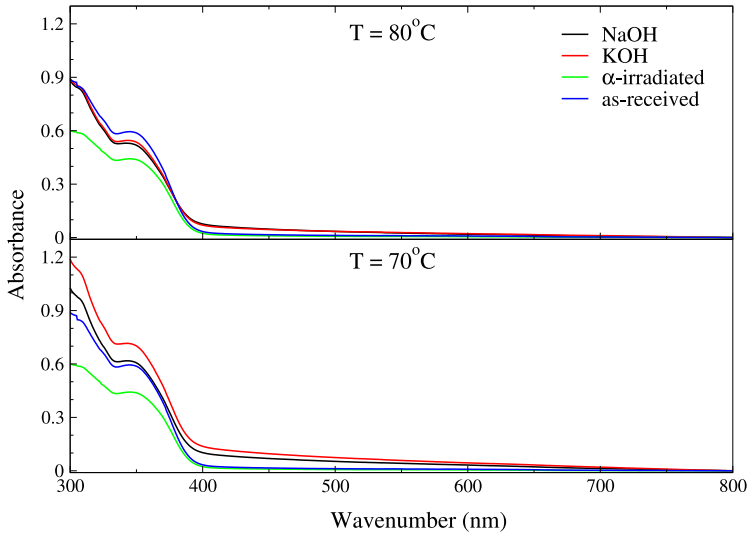

Fig. 6. Absorbance spectra in the ultraviolet and visible wavelength ranges were obtained for the as-received, only irradiated, and the samples subjected to irradiation followed by chemical etching. Two different chemical etching solutions, NaOH and KOH, were employed at temperatures of 80 °C (top) and 70 °C (bottom).

Table 5
The calculated direct band-gap energy (Eg) using the Tauc equation (Wood and Tauc, 1972) for the Durolon® polymer.

Samples	Eg (eV)
as-received	3.222 ± 0.013
irradiated	3.216 ± 0.032
KOH-70	3.186 ± 0.025
KOH-80	3.202 ± 0.016
NaOH-70	3.191 ± 0.013
NaOH-80	3.196 ± 0.019

method (Mooney and Kambhampati, 2013) was used to convert the absorbance spectra from wavelength units to energy units.

The calculated direct band-gap energies for the as-received, only irradiated, and irradiated-etched samples ranged from 3.18 eV to 3.22 eV. These results indicate that, regardless of the irradiation and etching conditions, there was no significant effect on the band-gap of the material.

The Raman and UV–vis results suggest that the affected volume by exposure and etching in the detectors was relatively minor compared to their original or overall volume. Therefore, these analyses indicates the formation of surface tracks by low-energy alpha particles in the Durolon® samples, agreeing with superficial densities observed in the etch pits analysis.

5. Conclusion

The efficiency of the Durolon® polymer for detecting alpha particles in the energy range of approximately 1–2 MeV was investigated, along with its dependence on chemical etching time using two different etching solutions (KOH or NaOH dissolved in an ethyl alcohol solution) at two different temperatures (70 and 80 °C).

To interpret the experimental data of track diameters, a phenomenological semi-empirical model was employed, which provided a good fit. The model follows the standard track modeling procedure (Somogyi and Szalay, 1973) but introduces a new V-function. The model was developed for normal incidence particle tracks, under the hypothesis that the etching velocity in the track direction was constant for the most part of its etchable range with a gradual transition to the bulk etching velocity near the end of the track. In practice, tracks in a range of track directions were considered. To adapt the model, a scale factor was introduced. Even with this caveat, the semi-empirical model made it possible to relate details of a proposed track geometry with observed etch pit diameter growth curves. Future work on this modeling could involve exploring different V-functions and applying the model to other detectors. Overall, this model offers practical applications for diameter variation calculations and experiment planning.

The results from Raman spectroscopy indicated that the chemical structures associated with the functional groups in the Durolon® polymer did not undergo significant degradation due to irradiation or etching processes. Similarly, UV–vis measurements revealed no substantial effects on the optical absorption bands of the material, irrespective of the irradiation and etching conditions. These findings suggested minimal volume impact on detectors from the exposure to low-fluency and low-energy alpha particles and etching, indicating the formation of surface tracks in Durolon® samples, consistent with observed superficial densities in the etch pits analysis. While the Raman and UV–vis studies did not show significant changes due to irradiation, they contribute to our understanding by ruling out certain possibilities and guiding future research directions.

Computational simulations were used to estimate the penetration of alpha particles into the Durolon® polymer, and the obtained value was found to be small. This finding aligns with the track density data, which showed a rapid decrease with increasing etching time. Thus, for low-energy alpha particle irradiations, the Durolon® polymer exhibits surface tracks and confirms its optical behavior in UV–vis measurements. Consequently, this polymer holds potential for detecting high-energy particle tracks that would generate deeper penetration, such as fission tracks. In summary, the Durolon® polymer has demonstrated promising nuclear track registration properties, particularly for low-energy alpha tracks. The results of this study highlight its potential as a track nuclear plastic detector.

CRediT authorship contribution statement

K.C.C. Pires: Writing – review & editing, Writing – original draft, Supervision, Project administration, Investigation, Conceptualization. **Y. Abuchaim:** Methodology, Data curation. **R. Künzel:** Writing – review & editing, Writing – original draft, Methodology, Formal analysis, Data curation. **S. Guedes:** Writing – review & editing, Project administration, Investigation, Formal analysis, Conceptualization. **M. Assunção:** Writing – original draft, Supervision, Investigation, Conceptualization. **N.M. Trindade:** Writing – review & editing, Writing – original draft, Validation, Formal analysis. **R.R. Aquino:** Resources, Data curation. **O.C.B. Santos:** Writing – original draft, Investigation, Formal analysis.

Declaration of competing interest

The authors declare that they have no known competing financial interests or personal relationships that could have appeared to influence the work reported in this paper.

Data availability

Data will be made available on request.

Acknowledgments

The authors would like to thank the Conselho Nacional de Desenvolvimento Científico e Tecnológico (CNPq/MCTI) grants #308192/2019-2, #409338/2021-4, #309489/2021-0 and #306929/2022-8; São Paulo Research Foundation (FAPESP) grants #2019/07767-1, #2018/05982-0 and #2021/12254-3, INCT-FNA project no. 464898/2014-5 and the University of São Paulo for the financial support. The authors would like to extend special thanks to S. C. Pires (*in memoriam*) for their invaluable support in the chemistry laboratory.

References

Aquilanti, V., Mundim, K.C., Elango, M., Kleijn, S., Kasai, T., 2010. Temperature dependence of chemical and biophysical rate processes: Phenomenological approach to deviations from Arrhenius law. Chem. Phys. Lett. 498 (1), 209–213. http://dx.doi.org/10.1016/j.cplett.2010.08.035.

Araújo, E.S., Khoury, H.J., Silveira, S.V., 1998. Effects of gamma-irradiation on some properties of durolon polycarbonate. Radiat. Phys. Chem. 53 (1), 79–84. http://dx.doi.org/10.1016/s0969-806x(97)00300-9.

Artham, T., Doble, M., 2008. Biodegradation of aliphatic and aromatic polycarbonates. Macromol. Biosci. 8 (1), 14–24. http://dx.doi.org/10.1002/mabi.200700106.

Balestra, S., Cozzi, M., Giacomelli, G., Giacomelli, R., Giorgini, M., Kumar, A., Mandrioli, G., Manzoor, S., Margiotta, A.R., Medinaceli, E., Patrizii, L., Popa, V., Qureshi, I.E., Rana, M.A., Sirri, G., Spurio, M., Togo, V., Valieri, C., 2007. Bulk etch rate measurements and calibrations of plastic nuclear track detectors. Nuclear Instruments & Methods in Physics Research Section B-Beam Interactions with Materials and Atoms 254 (2), 254–258. http://dx.doi.org/10.1016/j.nimb.2006.11.056.

Cassou, R., Benton, E.V., 1978. Properties and applications of CR-39 polymeric nuclear track detector. Nucl. Track Detect. 2, 173–179. http://dx.doi.org/10.1016/0145-224X(78)90021-2.

Chen, J.-H., Lin, J.-N., Kang, Y.-M., Yu, W.-Y., Kuo, C.-N., Wan, B.-Z., 2005. Preparation of nano-gold in zeolites for CO oxidation: Effects of structures and number of ion exchange sites of zeolites. Appl. Catal. A: General 291 (1), 162–169. http://dx.doi.org/10.1016/j.apcata.2005.02.038.

Cohen, E., Cvitas, T., Fry, J., et al., 2007. IUPAC Quantities, Units and Symbols in Physical Chemistry. IUPAC and RSC Publishing, Cambridge.

Delpech, M.C., Coutinho, F.M., Habibe, M.E.S., 2002. Bisphenol A-based polycarbonates: characterization of commercial samples. Polym. Test. 21 (2), 155–161. http://dx.doi.org/10.1016/s0142-9418(01)00063-0.

Dörschel, B., Bretschneider, R., Hermsdorf, D., Kadner, K., Kühne, H., 1999. Measurement of the track etch rates along proton and alpha particle trajectories in CR-39 and calculation of the detection efficiency. Radiat. Meas. 31 (1), 103–108. http://dx.doi.org/10.1016/S1350-4487(99)00117-1, Proceedings of the 19th International Conference on Nuclear Tracks in Solids.

Durolon, 2009. Unigel Plásticos, Datasheet manufacturer's catalog, Policarbonatos do Brasil S.A. Salvador URL: http://www.unigel.com.br/.

Dybal, J., Schmidt, P., Baldrian, J., Kratochvíl, J., 1998. Ordered structures in polycarbonate studied by infrared and Raman spectroscopy, wide-angle X-ray scattering, and differential scanning calorimetry. Macromolecules 31 (19), 6611–6619. http://dx.doi.org/10.1021/ma9807623.

Ferreira, T., Rasband, W., 2012. Programme ImageJ User Guide. URL: http://imagej.nih.gov/ij/index.html. (Accessed 08 October 2020).

Freitag, D., Grigo, U., Muller, P.R., Nouvertne, W., 1988. Polycarbonates, In: Mark, H.F., Bikales, N.M., Overberger, C.G., Menges, G. (Eds.), second ed. In: Encyclopedia of Polymer Science and Engineering, vol. 11, p. 648.

Fromm, M., Chambaudet, A., Membrey, F., 1988. Data bank for alpha particle tracks in CR-39 with energies ranging from 0.5 to 5.0 MeV recorded for various incident angles. Int. J. Rad. Appl. Instrum. D Nucl. Tracks Rad. Meas. 15 (1), 115–118. http://dx.doi.org/10.1016/1359-0189(88)90112-4, Special Volume Solid State Nuclear Track Detectors.

Gedler, G., Antunes, M., Velasco, J., 2013. Graphene-induced crystallinity of bisphenol A polycarbonate in the presence of supercritical carbon dioxide. Polymer 54 (23), 6389–6398. http://dx.doi.org/10.1016/j.polymer.2013.09.050.

Gupta, D., Kumar, S., Kalsi, P., Manchanda, V., Mittal, V., 2015. γ zieglerRay modifications of optical/chemical properties of polycarbonate polymer. World J. Condens. Matter Phys. 05, 129–137. http://dx.doi.org/10.4236/wjcmp.2015.53015.

Knoll, G.F., 2010. Radiation Detection and Measurement. John Wiley & Sons.

Lee, S.-N., Stolarski, V., Letton, A., Laane, J., 2000. Studies of bisphenol-A–polycarbonate aging by Raman difference spectroscopy. J. Mol. Struct. 521 (1–3), 19–24. http://dx.doi.org/10.1016/s0022-2860(99)00422-6.

Liu, H., Lin, S., Yu, N., 1990. Resonance Raman enhancement of phenyl ring vibrational modes in phenyl iron complex of myoglobin. Biophys. J. 57 (4), 851–856. http://dx.doi.org/10.1016/S0006-3495(90)82604-7.

Mooney, J., Kambhampati, P., 2013. Get the basics right: Jacobian conversion of wavelength and energy scales for quantitative analysis of emission spectra. J. Phys. Chem. Lett. 4, 3316–3318. http://dx.doi.org/10.1021/jz401508t.

Oliveira, C.S., Malheiros, B., Pires, K.C.C., Assunção, M., Guedes, S., Corrêa, J., Paschuk, S., 2021. Low energy alpha particle tracks in CR-39 nuclear track detectors: Chemical etching studies. Nucl. Instrum. Methods Phys. Res. A 995, 165130. http://dx.doi.org/10.1016/j.nima.2021.165130.

Pelletier, M.J., 2003. Quantitative analysis using Raman spectrometry. Appl. Spectrosc. 57 (1), 20A–42A. http://dx.doi.org/10.1366/000370203321165133.

Pugliese, F., 2008. Caracterização do polímero Durolon como detector de traços nucleares de estado sólido (Ph.D. thesis). Universidade de São Paulo.

Rahaman, M.H.A., Khandaker, M.U., Khan, Z.R., Kufian, M.Z., Noor, I.S.M., Arof, A.K., 2014. Effect of gamma irradiation on poly(vinyledene difluoride)–lithium bis(oxalato)borate electrolyte. Phys. Chem. Chem. Phys. 16 (23), 11527–11537. http://dx.doi.org/10.1039/c4cp01233j.

Rana, M.A., 2008. On problems in trustworthy predictions of etched track parameters. Radiat. Meas. 43 (9), 1546–1549. http://dx.doi.org/10.1016/j.radmeas.2008.09.002.

Rana, M.A., 2010. Systematic measurements of etch induction time for nuclear tracks: Startup of etching and the multiplex effect. Nucl. Instrum. Methods Phys. Res. A 618 (1), 176–181. http://dx.doi.org/10.1016/j.nima.2010.02.108.

Resta, V., Quarta, G., Lomascolo, M., Maruccio, L., Calcagnile, L., 2015. Raman and Photoluminescence spectroscopy of polycarbonate matrices irradiated with different energy ^{28}Si+ ions. Vacuum 116, 82–89. http://dx.doi.org/10.1016/j.vacuum.2015.03.005.

Silva, A.O., Kunzel, R., Yoshimura, E.M., Pires, K.C.C., Trindade, N.M., 2024. Optically stimulated luminescence of durolon polycarbonate. J. Lumin. 120613.. http://dx.doi.org/10.1016/j.jlumin.2024.120613.

Soares, C.J., Alencar, I., Guedes, S., Takizawa, R.H., Smilgys, B., Nadler, J.C., 2013. Alpha spectrometry study on LR115 and Makrofol through measurements of track diameter. Rad. Meas. 50, 246–248. http://dx.doi.org/10.1016/j.radmeas.2012.06.010.

Somogyi, G., Szalay, S.A., 1973. Track-diameter kinetics in dielectric track detectors. Nucl. Instrum. Methods 109 (2), 211–232. http://dx.doi.org/10.1016/0029-554x(73)90265-6.

Stuart, B.H., 1996. Temperature studies of polycarbonate using Fourier transform Raman spectroscopy. Polym. Bull. 36, 341–346. http://dx.doi.org/10.1007/BF00319235.

Wood, D.L., Tauc, J., 1972. Weak absorption tails in amorphous semiconductors. Phys. Rev. B 5, 3144–3151. http://dx.doi.org/10.1103/PhysRevB.5.3144.

Zimmerer, C., Matulaitiene, I., Niaura, G., Reuter, U., Janke, A., Boldt, R., Sablinskas, V., Steiner, G., 2019. Nondestructive characterization of the polycarbonate - octadecylamine interface by surface enhanced Raman spectroscopy. Polym. Test. 73, 152–158. http://dx.doi.org/10.1016/j.polymertesting.2018.11.023.